

Adaptive Tuned Vibration Absorbers: Design Principles, Concepts and Physical Implementation

Philip Bonello
University of Manchester
United Kingdom

1. Introduction

The tuned vibration absorber (TVA) has been used for vibration control purposes in many sectors of civil/automotive/aerospace engineering for many decades since its inception by (Ormondroyd & Den Hartog, 1928). A tuned vibration absorber (TVA), in its most generic form, is an auxiliary system whose parameters can be tuned to suppress the vibration of a host structure. The auxiliary system is commonly a spring-mass-damper system (or equivalent) and the TVA suppresses the vibration at its point of attachment to the host structure through the application of an interface force. The tuned frequency ω_a of the TVA is defined as its undamped natural frequency with its base (point of attachment) blocked. The TVA can be used in two distinct ways, resulting in different optimal tuning criteria and design requirements (von Flotow et al., 1994):

- a. It can be tuned to suppress (*dampen*) the modal contribution from a specific troublesome natural frequency Ω_s of the host structure over a wide band of excitation frequencies.
- b. It can be tuned to suppress (*neutralise*) the vibration at a specific troublesome excitation frequency ω , in which case it acts like a notch filter.

When used for application (a), the TVA referred to as a “tuned mass damper” (TMD). ω_a is optimally tuned to a value slightly lower than that of the targeted mode Ω_s and an optimal level of damping needs to be designed into the absorber. When used for application (b), the TVA is referred to as a “tuned vibration neutraliser” (TVN) (Brennan, 1997, Kidner & Brennan, 1999) or “undamped TVA”. The optimal tuning condition is in this case is $\omega_a = \omega$ and the TVN suppresses the vibration over a very narrow bandwidth centred at the tuned frequency. Total suppression of the vibration at this frequency is achieved when there is no damping in the TVN.

Deviation from the tuned condition (mistuning) degrades the performance of either variant of the TVA (von Flotow et al., 1994) and it can be shown that a mistuned vibration neutraliser could actually increase the vibration of its host structure (Brennan, 1997). To avoid mistuning, smart or adaptive tunable vibration absorbers (ATVAs) have been developed. Such devices are capable of retuning themselves in real time. Adaptive technology is especially important in the case of the TVN since the low damping requirement in the spring element can raise the host structure vibration to dangerous levels

in the mistuned condition. In this case, mistuning can occur either due to a drift in the forcing frequency or due to a drift in tuned frequency caused by environmental factors (e.g. temperature change). Hence, a TVN needs to be adaptive to be practically useful.

At the heart of an ATVA is a means for adjusting the tuned frequency ω_a in real time. This is frequently done through the variation of the effective mechanical stiffness of the ATVA, although other means are possible. Whatever the retuning method used, the device should be tunable over an adequate range of frequencies, and the adjustment should be rapid and with minimum power requirement. The device must also be cheap and easy to manufacture. To maximise vibration attenuation, the retuning mechanism should add as little as possible to the redundant mass of the device and, in the case of the neutraliser, have a low structural damping (Brennan, 1997). The technical challenge is to design an adaptive device with such attributes.

This chapter continues with a quantitative illustration of the basic design principles of both variants of the TVA. It will then present a comprehensive review of the various design concepts that have been presented for the ATVA, including the latest innovations contributed by the author. This section will cover the use of piezoelectric actuators, shape-memory alloys and servo-actuators within the smart structure of the ATVA. Control algorithms and their implementation through MATLAB® with SIMULINK® will also be discussed.

2. Basic design principles of TVA

With reference to Fig. 1a, the above-defined frequency ω_a coincides exactly with the lowest anti-resonance frequency of the attachment point receptance frequency response function (FRF) of the undamped “free-body” TVA structure, $r_{AA}(\omega) = Y_A/F$, where Y_A and F are complex amplitudes of y_A and the interface force $f(t)$, for harmonic vibration at circular frequency ω . It is for this reason that, for the TVN, the condition $\omega_a = \omega$ defines optimal tuning. For excitation frequencies ω below the first non-zero resonance frequency ω_m of $r_{AA}(\omega)$, the absorber can be represented by the equivalent two-degree-of-freedom model shown in Fig. 1b (Bonello & Groves, 2009). Fig. 1b shows that the absorber mass m_a is split into an effective mass $m_{a,eff} = Rm_a$ and a redundant mass $m_{a,red} = (1-R)m_a$. The latter mass simply adds to the host structure. The effective part of the absorber is the single-degree-of-freedom system constituted by mass $m_{a,eff}$, the spring of stiffness $k_a = \omega_a^2 m_{a,eff}$ and a damping element. In the case of a TMD, where damping is deliberately designed into the device, it is preferable to represent it by viscous damper of frequency-independent coefficient c_a . In the case of a TVN, where the damping is an unwanted inherent feature of the spring element, it is best represented by a structural damping mechanism of loss factor η_a , for which the equivalent viscous damping coefficient is $k_a \eta_a / \omega$. The method for deriving the equivalent two-degree-freedom is detailed in Section 4.1.

2.1 Tuned mass damper

The purpose of the TMD is to dampen a particular resonance peak of the FRF $r_{AP}(\omega)$ connecting the response at A to an external force $f_p(t)$ applied to the host structure at some arbitrary point P. It is useful for applications where the excitation has a broad frequency spectrum containing the targeted mode. The damping in the original host structure (i.e. the

structure prior to the addition of the TMD) is commonly assumed to be negligible relative to that introduced by the TMD. Suppose the TMD is targeted at the s^{th} mode of the original host structure. Let Ω_s be the frequency of this mode and $\psi_A^{(s)}$ denote the value of the corresponding mass-normalised mode-shape at the degree of freedom being targeted (e.g. the vertical displacement at A in Fig. 1). Then, from standard modal theory (Ewins, 1984), the contribution of the targeted mode to the dynamics of the original host structure at the targeted degree of freedom can be represented as the simple mass-spring system of mass $M_A^{(s)} = 1/\{\psi_A^{(s)}\}^2$ and stiffness $K_A^{(s)} = \Omega_s^2 M_A^{(s)}$ (see Fig. 2(a)). The dynamics of the original host structure at the targeted degree of freedom can be accurately modelled in this form for excitation frequencies ω in the vicinity of Ω_s , where the targeted mode is dominant. Addition of the TMD in Fig. 1b to the system in Fig. 2(a) results in the system in Fig. 2(b). Notice that original host structure modal mass $M_A^{(s)}$ needs to be readjusted to $M_A^{(s)} + m_{a,red}$, to account for the addition of the redundant absorber mass to the host structure. The harmonic analysis of the systems in Figs. 2(a,b) (i.e. analysis with $f_p = \text{Re}\{F_p e^{j\omega t}\}$) then gives a modal approximation of $r_{AP}(\omega)$, denoted by $r_{AP}^{(s)}(\omega)$, which is accurate for frequencies ω in the vicinity of Ω_s .

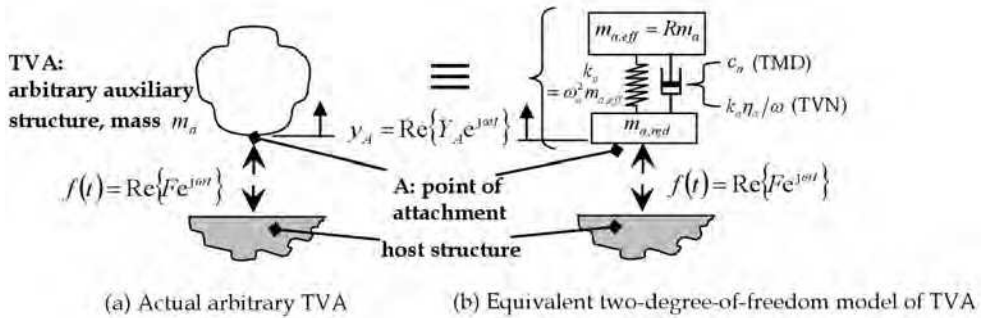


Fig. 1. Generic TVA

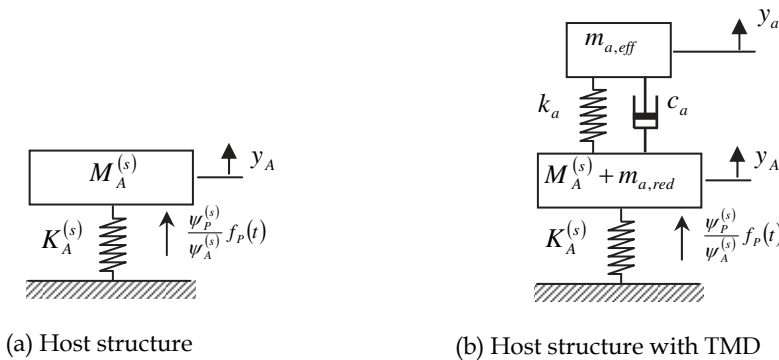


Fig. 2. Dynamic modal model of the host structure without/with TMD for frequencies ω in the vicinity of Ω

$r_{AP}^{(s)}(\omega)$ can be dampened by adapting the harmonic analysis in (Den Hartog, 1956) to the system in Fig. 2(b). The optimal tuning condition is found to be:

$$\frac{\omega_{opt}}{\Omega'_s} = \frac{1}{1 + \mu} \quad (1)$$

where

$$\Omega'_s = \Omega_s \sqrt{M_A^{(s)} / \{M_A^{(s)} + m_{a,red}\}}, \quad \mu = m_{a,eff} / \{M_A^{(s)} + m_{a,red}\} \quad (2)$$

The viscous damping coefficient is given by:

$$c_a = 2\zeta_a m_{a,eff} \omega_a \quad (3)$$

The optimal value of the viscous damping ratio ζ_a is given by (Den Hartog, 1956):

$$\zeta_{a,opt} = \sqrt{\frac{3\mu}{8(1 + \mu)^3}} \quad (4)$$

The optimisation of the modulus of $r_{AP}^{(s)}(\omega)$ is illustrated in Fig. 3. The introduction of the TMD splits the original host structure resonance peak into two peaks separated by an anti-resonance. Points M and N are referred to as the 'fixed points' since, for given μ and ω_a , the function $|r_{AP}^{(s)}(\omega)|$ of the modified structure passes through them regardless of the value of ζ_a . The optimal tuning condition of eq. (1) ensures that the fixed points are level with each other (this is the case illustrated in Fig. 3). With this condition in place, the optimal damping condition of eq. (4) ensures that the peaks of $|r_{AP}^{(s)}(\omega)|$ coincide as closely as possible with the fixed points. The height of these optimised peaks is approximately inversely proportional to $\sqrt{\mu}$.

As an illustration of the effect of a TMD on a multimodal (i.e. continuous) system, consider a TMD attached to the tip of a cantilever and tuned to attenuate its second flexural mode (Fig. 4). The cantilever OA is of length 1m and made of steel (Young Modulus 200 GN/m², density 7850 kg/m³) of circular section with diameter 3cm.

Assuming an Euler-Bernoulli beam model, an eigenvalue analysis yields $\Omega_2/(2\pi) = 132.8$ Hz, $M_A^{(2)} = 1.387$ kg. The mass ratio μ is taken as 2%. For simplicity, the TMD is assumed to have no redundant mass. The TMD parameters were computed according to the above formulae. The receptances $r_{AP}(\omega) = Y_A/F_P$ of the system with and without the TMD were evaluated using the Dynamic Stiffness Method (Bonello & Brennan, 2001) and shown in Fig. 5, where the dampening of the targeted resonance is clearly evident.

Fig. 6 illustrates the effect of mistuning i.e. deviation from the tuned condition of eq. (1). The stiffness k_a of the TMD was varied such that it was mistuned by 10% i.e. ω_a was set to $1.1\omega_{a,opt}$, with c_a kept the same as the optimal case of Fig. 5 (considering eqs. (3) and (4), this means that ζ_a of the mistuned case in Fig. 6 is not $\zeta_{a,opt}$). It is clear from Fig. 6 that a slight mistuning produces significant deterioration of the TMD performance.

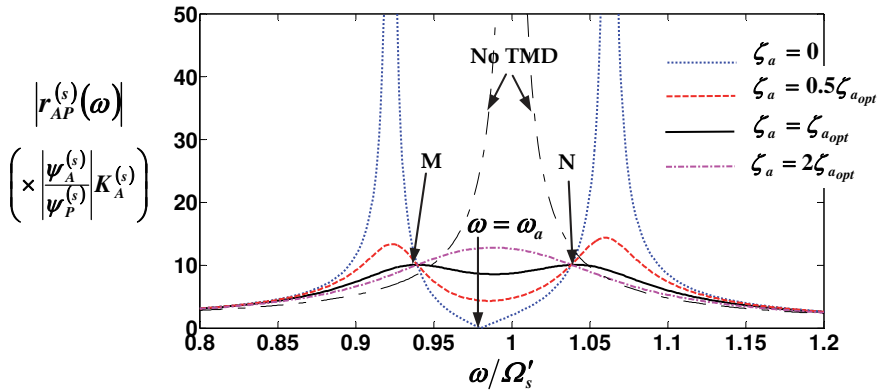


Fig. 3. Effect of damping on the modal approximation of the attachment point FRF (case shown is for the tuned condition, eq. (1), with $\mu = 0.02$)

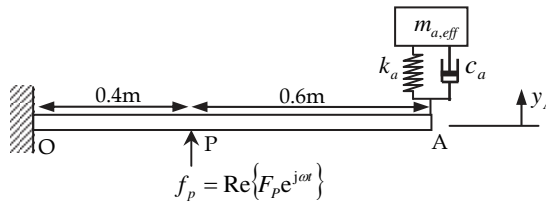


Fig. 4. TMD attached to a cantilever

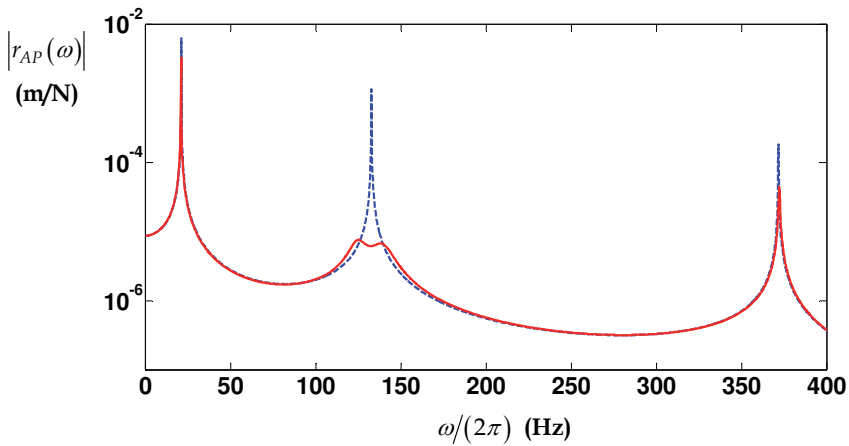


Fig. 5. Effect of TMD targeted against the second flexural mode of cantilever in Figure 4: original system (dashed line); with TMD (solid line)

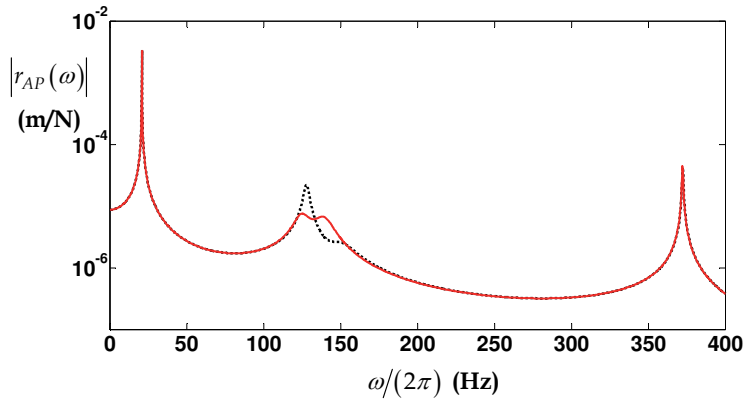


Fig. 6. Effect of a mistuned TMD on cantilever in Figure 4: TMD optimally tuned and damped as per eqs. (1) and (4) (solid line); 10% mistuned TMD (dotted line)

Finally, it is worth mentioning that a similar effect to the TMD can be achieved through an electrical analogue, wherein the auxiliary system is a piezoelectric shunt circuit (Park, 2002). In such an 'electrical' TVA, a piezoelectric patch is bonded to the host structure and connected across an external inductor-resistor circuit. The piezoelectric patch is used to convert the vibration energy of the host structure into electrical energy and introduces a capacitor effect into the circuit, turning it into an L-C-R circuit. The electrical energy is then dissipated most efficiently as heat through the resistor when the electrical resonance produced by the LC components is close to the frequency of the targeted mode and the resistor has an optimum value. One major disadvantage of the electrical TVA is the difficulty in deriving the transfer function of the modified system (on which the optimisation is based); the difficulty increases with the complexity of the host structure. For this reason the electrical TVA has typically been restricted to simple host structures like cantilevers (e.g. Park, 2002). In contrast, the classical theory of the mechanical TMD is readily applicable to any arbitrary host structure since the only host structure data it requires are the frequency and modal mass of the targeted mode.

2.2 Tuned vibration neutraliser

The purpose of the TVN is to plant an anti-resonance in the FRF $r_{AP}(\omega)$ at some particular chosen value of the excitation frequency ω . Hence, the TVN is typically used for applications where the excitation is entirely, or mainly, at a single frequency (i.e. harmonic). For example, suppose that it is required to cancel the tip vibration of the above considered cantilever (Fig. 4) at a frequency of 50 Hz. The optimal condition for a TVN is

$$\omega_a = \omega \quad (5)$$

Hence, in this example, ω_a is optimally set to 100π . Neglecting the redundant TVA mass and assuming an effective mass of the absorber, the absorber stiffness is calculated accordingly. The effect of the TVN is illustrated in Fig. 7, where the absorber mass is assumed to be 2% of the total mass of the beam. It is seen that an anti-resonance is introduced at the desired frequency, in addition to a resonance at a slightly higher

frequency (52 Hz) (the difference between the anti-resonance and resonance frequencies is found to increase with the effective TVN mass).

(Brennan, 1997) defines the attenuation D provided by a TVN for harmonic excitation as the ratio of the vibration amplitude at A without the TVN to the amplitude there with the TVN attached and optimally tuned:

$$D = \frac{|Y_A|_{\text{free}}}{|Y_A|_{\text{TVN, opt}}} \tag{6}$$

In the absence of damping in the absorber $D \rightarrow \infty$ (complete attenuation). The attenuation degrades with increasing absorber damping η_a (since this reduces the depth of the anti-resonance in Fig. 7). Also, for given absorber damping, the TVA’s attenuating capability degrades as $m_{a,eff}$ is reduced. In fact, for a host structure that is a rigid machine of mass M mounted on soft isolators, (Brennan, 1997) showed that

$$D \approx \mu / \eta_a \tag{7}$$

where

$$\mu = m_{a,eff} / (M + m_{a,red}) \tag{8}$$

Deviation from the optimally tuned condition $\omega_a = \omega$ (mistuning) can occur due to a change in the excitation frequency (e.g. a change in operating speed of rotating machinery). It is evident from Fig. 7 that even a slight mistuning will drastically degrade the performance of the TVN. In fact, as can be seen in Fig. 7, if the excitation frequency drifts above ω_a then the vibration neutraliser actually increases the vibration of its host structure due to the extra resonance it introduced into the system. This extra resonance is itself made more pronounced by the low damping requirement.

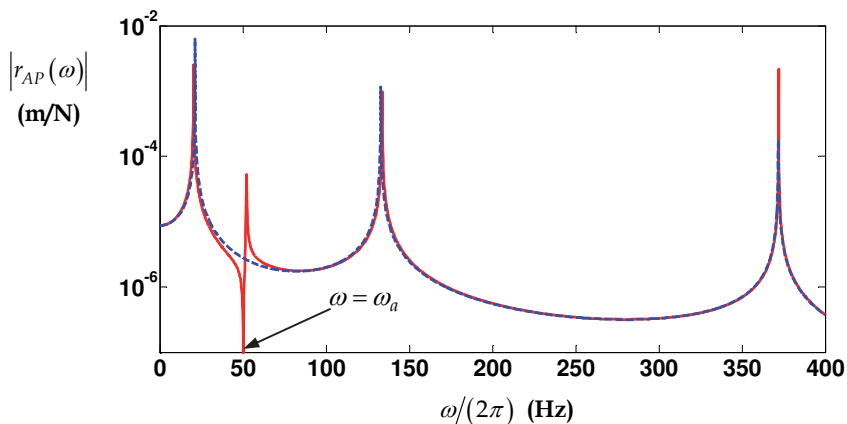


Fig. 7. Effect of TVN tuned to an excitation frequency of 50Hz on the cantilever in Fig. 4: original system (dashed line); with TVN (solid line)

3. Adaptive tuned vibration absorbers – an overview

“Tuning” a TVA involves making the appropriate adjustment of ω_a and this is done through an adjustment in one or more properties of the TVA structure. Mistuning is avoided through the use of adaptive (or “smart”) tuneable vibration absorbers (ATVAs) which can automatically perform the necessary adjustment in real time (von Flotow et al., 1994, Brennan et al., 2004a). As demonstrated in the previous section, mistuning is a far more serious issue for the TVN, since the requirement for low absorber damping can raise the host structure vibration to dangerous levels in the mistuned condition. It is for this reason that adaptive technology has been mainly developed in the context of the TVN. *The ATVAs considered in the remainder of the chapter will therefore exclusively be vibration neutralisers.*

In the context of the TVN, adaptive tuning of the device involves maintaining the condition $\omega_a = \omega$ in the presence of variable conditions (typically a time-varying excitation frequency ω , in which case the antiresonance in Fig. 7 is shifted in real time along the frequency axis, in accordance to the current value of the excitation frequency). The challenge for ATVA designers is to produce a device with the following attributes:

- i. low structural damping;
- ii. any actuating mechanism to retune the device should add as little as possible to the redundant mass;
- iii. the device should be tuneable over a wide range of frequencies;
- iv. retuning should be rapid and with minimum power requirement;
- v. the device should be cheap and easy to design and manufacture.

Various design concepts for ATVAs have been proposed (von Flotow et al., 1994, Brennan et al., 2004a). One early variable stiffness element used in a vibration absorber was described in (Longbottom et al., 1990). A mass was sandwiched between a pair of pneumatic rubber bellows (Fig. 8) and the stiffness was adjusted by changing the air pressure inside the bellows. Further work on this device by (Long et al., 1998) resulted in a means of automatically adjusting the stiffness. However, the high amount of damping introduced by the rubber bellows was a major disadvantage.

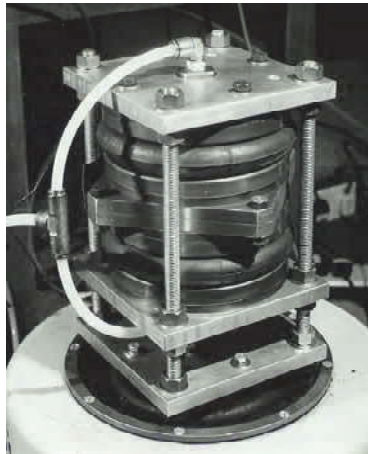


Fig. 8. Pneumatic rubber bellows ATVA (Brennan et al., 2004b)

One recent strategy for adaptation, by (Rustighi et al., 2005), was to utilise the variation with temperature of the Young Modulus of a beam-like ATVA made of a shape memory alloy (SMA) conductor (Fig. 9). The SMA wire formed a double cantilever, projecting from either side of the central attachment point to the host structure. The ATVA stiffness was controlled by adjusting the current through the wire. Despite being strong in attributes (i), (ii) and (v) above, this device could only achieve a maximum variation of around 20% in tuned frequency, taking as long as 2 minutes with a 9A current to do so (Brennan et al., 2004a, Rustighi et al., 2005).

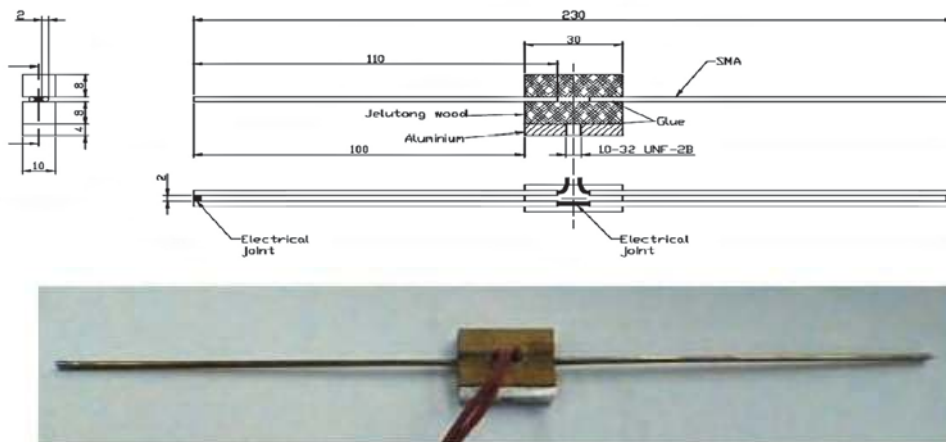


Fig. 9. Shape memory alloy ATVA (Rustighi et al., 2005)

Another recent approach, by (Bonello et al., 2005) was to utilise a mass-spring ATVA in which the stiffness element was composed of parallel curved beams in longitudinal compression (Fig. 10). The longitudinal stiffness was controlled by adjusting the curvature through piezo-ceramic actuators bonded to the beams. This device was capable of very rapid tuning over a frequency range 36-56 Hz (56% variation). However, this design concept was inherently limited to low frequency applications as a result of inertia effects in the curved beams (Bonello et al., 2005).

Other works have focused on the use of a beam-like ATVA controlled through servo-actuation. This concept remains the best approach for applications requiring a wide tuning frequency range (Carneal et al., 2004). Figs. 11-15 show various such ATVA designs. The "moveable-supports" ATVA in Fig. 11 was patented by (Hong & Ryu, 1985). It consisted of a beam with a mass attached to its centre and supports that could be moved relative to each other, thereby altering ω_d .

(Brennan, 2000) performed a theoretical study of the tuning frequency characteristics of the designs in Figs. 12, 13. In Fig. 12, the ATVA beam is composed of two beams and the effective stiffness of the ATVA is adjusted by pushing apart the two constituent beams at the centre, thereby altering the ATVA beam cross-section. Such a device was built and tested in (Kidner et al., 2002), where a maximum adjustment of 35% in tuned frequency was achieved. This concept appears to provide the most rapid tuning of all beam-like designs in Figs. 11-15 since the actuator is required to move the least distance to achieve a given change

in ω_a . However, the actuator has to work against much larger forces and the variability in ω_a is clearly limited by the maximum deformation that the constituent beams can withstand as they are being prised apart. Through elementary analysis, (Brennan, 2000) predicted that a considerably greater tuning range is achievable through the two alternative designs in Fig. 13 (“moveable beam” or “moveable masses”). In the “moveable beam” approach the masses are fixed relative to the beam and the beam lengthens or shortens. This device does not appear to have been built and would require some form of telescoping beam. The “moveable-masses” concept is more feasible: the beam is of fixed length and tuning is achieved by repositioning the attached masses. (Von Flotow et al., 1994) describes devices that appear to match this latter description in operation on the Boeing Chinook helicopter, although the details available are very sketchy.

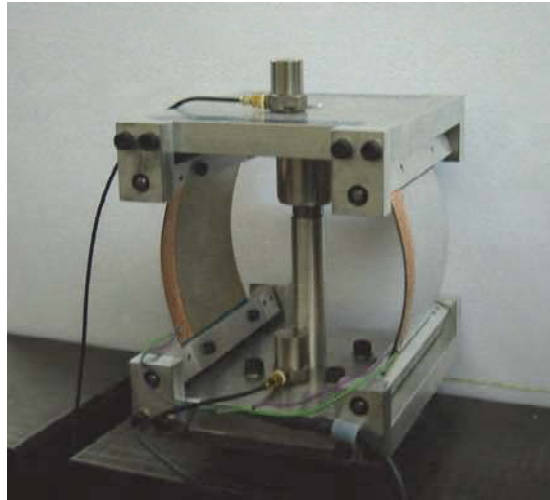


Fig. 10. ATVA with variable-curvature piezo-actuated beams (Bonello et al., 2005)

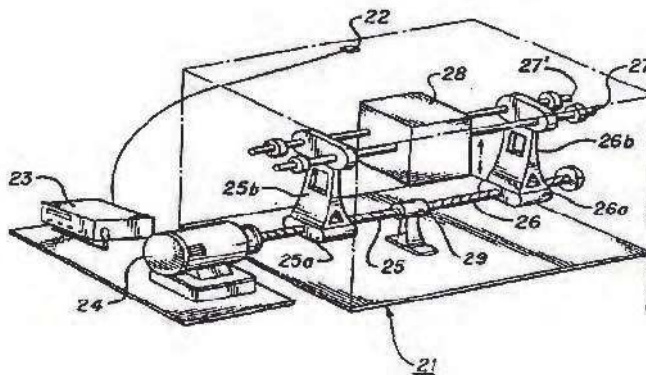


Fig. 11. Servo-actuated beam ATVA: moveable-supports, conventional design (Hong & Ryu, 1985)

In all devices of Figs. 11-13, the actuator is a permanently redundant mass that degrades the attenuating capacity of the ATVA (eq. (7, 8)). This limitation was overcome by (Carneal et al., 2004) who improved the “moveable-supports” concept of (Hong & Ryu, 1985) by incorporating the actuator into the central mass supported by the beam (Fig. 14). This necessitated the use of a “V-Type” undercarriage. The design of this undercarriage (and the one used in Fig. 11) clearly warrants careful consideration. It should be sufficiently rigid so as to avoid introducing unwanted dynamics that would interfere with ATVA operation. Moreover, it needs to be as light as possible to minimise the redundant mass. A far simpler approach would be to utilise a moveable-masses ATVA with actuators incorporated into the masses, as illustrated in Fig. 15, where the device simply attaches directly to the host structure at its centre. Such a novel device was proposed by (Bonello & Groves, 2009). Apart from the constructional simplicity, this concept was shown to provide superior ATVA performance. Another important contribution of (Bonello & Groves, 2009) was the derivation of the effective mass and tuned frequency characteristics of the moveable-supports and moveable-masses ATVA. This enables the designer to quantify their expected performance for any given application. The derivation of the effective mass of the beam-like ATVAs in Figs. 11-15 requires the derivation of their equivalent two-degree-of-freedom model (Fig. 1b). Such analysis is very important when one considers that, for the devices in Fig. 11-15 (with the possible exception of Fig. 12), the effective mass proportion R will vary as the ATVA is retuned. Although (Carneal et al., 2004) describe their actuator-incorporated mass (Fig. 14) as the “active mass” of the absorber, its degree of activity is actually dependent on the setting of the ATVA. The same can be said of the moveable-masses concept (Fig. 15). With the supports or masses fully retracted in Figs. 14 and 15, the attached masses clearly become entirely redundant and the effective mass proportion R in Fig. 1b is then entirely contributed by the beam itself. This means that, as the ATVA retunes itself, the attenuation it provides will vary due to the consequent variation in μ (eqs. (7, 8)). Hence, the knowledge of an “effective mass characteristic” of a moveable-supports or moveable-masses ATVA is important since it would allow the designer to quantify the expected attenuation provided by an ATVA over a range of frequencies for any given application.

4. ATVA analysis

The aims of this section are two-fold: (i) to illustrate the derivation of the effective mass and tuned frequency characteristics of moveable-supports and moveable-masses ATVAs (Figs. 14 and 15); (ii) to illustrate the physical implementation and testing of the beam-like ATVA with actuator-incorporated moveable masses (Fig. 15). This latter covers the adaptation logic control. The material in this section is based on the work in (Bonello & Groves, 2009), from which further details can be obtained.

4.1 Effective mass and tuned frequency characteristics

Fig. 16 shows the two alternative types of ATVA considered. It shall be assumed that the beam supports of the device in Fig. 16b are simple supports. Let A denote the point/points of attachment of the beam to the host structure and B denote the point/points of attachment of the mass/masses. The aim of the following analysis is the determination of the fractional change in tuned frequency ω_n and the variation of the effective mass proportion R (Fig. 1b) as the setting $\tilde{x} = x/L$ of the actual systems in Fig. 16 is varied. Hence, for this purpose, damping can be omitted from the analysis without loss of accuracy.

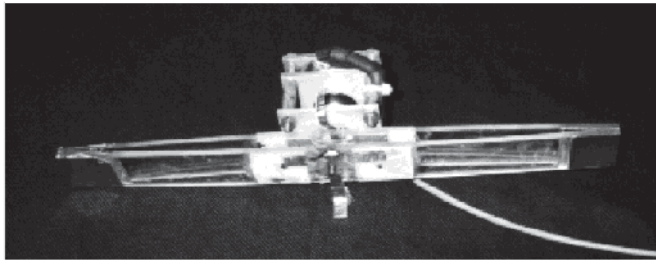
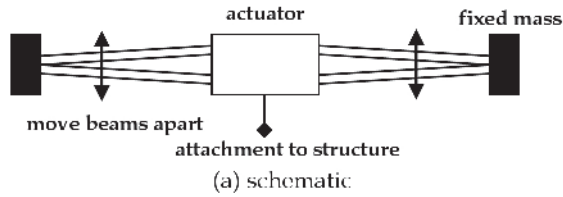


Fig. 12. Servo-actuated beam-like ATVA: adjustable beam-cross-section ATVA (Brennan, 2000, Kidner et al., 2002)

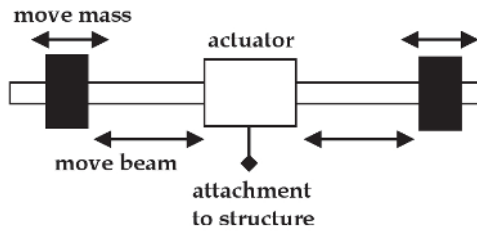


Fig. 13. Servo-actuated beam-like ATVA: moveable-beam or moveable-masses ATVA (Brennan, 2000)

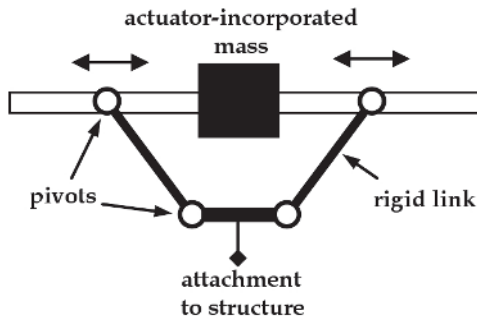


Fig. 14. Servo-actuated beam-like ATVA: moveable supports, “V-Type” design ATVA (Carneal et al., 2004)

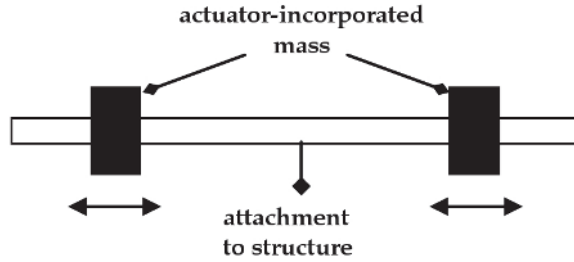


Fig. 15. Servo-actuated beam-like ATVA: actuator-incorporated moveable masses ATVA (Bonello & Groves, 2009)

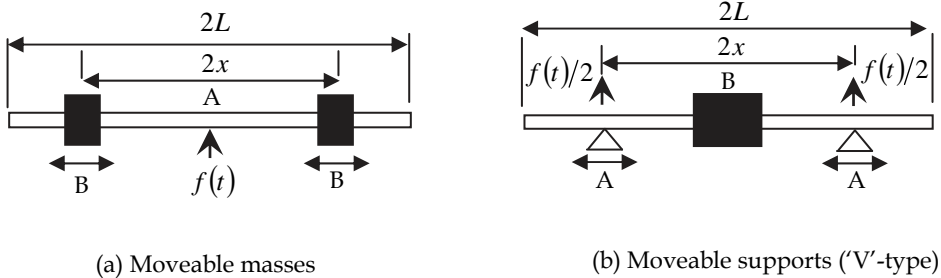


Fig. 16. Free-body schematics of two alternative designs for an actuator-incorporated mass ATVA

In either case the system will be regarded as comprising a beam acted upon by: (i) the reaction forces from the lumped mass attachments at B; (ii) the reaction force from the host. If the latter force is $f(t) = \text{Re}\{F e^{i\omega t}\}$, then the response at any point Q on the beam is $y_Q(t) = \text{Re}\{Y_Q e^{i\omega t}\}$. Following the analysis in (Bonello & Groves, 2009), the expression for the receptance of the TVA at its point of attachment to the structure is:

$$r_{AA}(\omega) = \frac{Y_A}{F} = \frac{[1 - \tilde{\omega}^2]}{m_b \omega_1^2} \left(\frac{\left[-\frac{1}{\tilde{\omega}^2} + \tilde{\beta}_{AA}(\tilde{\omega}) \right] \left[1 + \sigma - \sigma \tilde{\omega}^2 \tilde{\beta}_{BB}(\tilde{\omega}) \right] + \left[-\frac{1}{\tilde{\omega}^2} + \tilde{\beta}_{BA}(\tilde{\omega}) \right] \left[-\sigma + \sigma \tilde{\omega}^2 \tilde{\beta}_{AB}(\tilde{\omega}) \right]}{\left[1 - \tilde{\omega}^2 \right] \left[1 + \sigma - \sigma \tilde{\omega}^2 \sum_{k=3,5,\dots}^K \frac{\{\phi_B^{(k)}\}^2}{\tilde{\omega}_k^2 - \tilde{\omega}^2} \right] - \sigma \tilde{\omega}^2 \{\phi_B^{(1)}\}^2} } \right) \quad (9)$$

where:

$$\sigma = \frac{m_{att}}{m_b}, \quad \tilde{\omega} = \frac{\omega}{\omega_1}, \quad \tilde{\omega}_k = \frac{\omega_k}{\omega_1}, \quad \tilde{\beta}_{QS}(\tilde{\omega}) = \sum_{k=1,3,5,\dots}^K \frac{\phi_Q^{(k)}\phi_S^{(k)}}{\tilde{\omega}_k^2 - \tilde{\omega}^2} \quad (10a-d)$$

In the above expressions m_{att} is the sum of the attached masses at B (for moveable masses) or simply the mass at B (for moveable supports) and m_b is the mass of the beam alone. $\phi_Q^{(k)}$, $\phi_S^{(k)}$ are the k^{th} flexural non-dimensional mode-shape functions evaluated at arbitrary points Q, S and ω_k is the k^{th} flexural natural frequency. These modal parameters pertain to the *plain* beam (i.e. without lumped mass attachment) under free-free conditions. Notice that only the symmetric modes are considered due to the symmetry of the systems in Fig. 16. The expression in eq. (9) is exact for $K \rightarrow \infty$ but, for a given upper limit of the non-dimensional excitation frequency $\tilde{\omega}$, will be virtually exact for a sufficiently large finite value of K (corresponding to a total of $(K+1)/2$ symmetric modes). For the moveable masses absorber, $\phi_A^{(k)}$ is fixed and $\phi_B^{(k)}$ is variable; for the moveable supports absorber $\phi_B^{(k)}$ is fixed and $\phi_A^{(k)}$ is variable. If the Euler-Bernoulli beam model is assumed, then the free-free mode-shape function values tabulated by (Bishop & Johnson, 1960) can be used. In this case, from eq. (9), it is clear that the non-dimensional receptance function

$$\tilde{r}_{AA}(\tilde{\omega}, \tilde{x}, \sigma) = m_b \omega_1^2 r_{AA}(\omega) \quad (11)$$

is totally independent of the actual material and geometrical properties for either ATVA in Fig. 16.

For given \tilde{x} and σ , the lowest non-dimensional anti-resonance $\tilde{\omega}_a = \omega_a/\omega_1$ (i.e. the tuned frequency of the device) is obtained by finding the lowest value of $\tilde{\omega}$ for which the numerator of eq. (9) is 0:

$$\left[-\frac{1}{\tilde{\omega}^2} + \tilde{\beta}_{AA}(\tilde{\omega}) \right] \left[1 + \sigma - \sigma \tilde{\omega}^2 \tilde{\beta}_{BB}(\tilde{\omega}) \right] + \left[-\frac{1}{\tilde{\omega}^2} + \tilde{\beta}_{BA}(\tilde{\omega}) \right] \left[-\sigma + \sigma \tilde{\omega}^2 \tilde{\beta}_{AB}(\tilde{\omega}) \right] = 0 \quad (12)$$

Similarly, the lowest non-dimensional resonance $\tilde{\omega}_m = \omega_m/\omega_1$ is obtained by finding the lowest value of $\tilde{\omega}$ for which the denominator of eq. (9) is 0:

$$\left[1 - \tilde{\omega}^2 \right] \left[1 + \sigma - \sigma \tilde{\omega}^2 \sum_{k=3,5,\dots}^K \frac{\left\{ \phi_B^{(k)} \right\}^2}{\tilde{\omega}_k^2 - \tilde{\omega}^2} \right] - \sigma \tilde{\omega}^2 \left\{ \phi_B^{(1)} \right\}^2 = 0 \quad (13)$$

For any given K , the frequencies $\tilde{\omega}_a$, $\tilde{\omega}_m$ can be found by an iteration technique using as initial approximations the corresponding roots $\tilde{\omega}_a|_{K=1}$, $\tilde{\omega}_m|_{K=1}$ obtained for $K=1$. From eqs. (12, 13) it can be shown that:

$$\tilde{\omega}_a|_{K=1} = \frac{1}{\sqrt{1 + (1 + \sigma)\phi_A^2 + \sigma(\phi_B^2 - 2\phi_A\phi_B)}}, \quad \tilde{\omega}_m|_{K=1} = \sqrt{\frac{1 + \sigma}{1 + \sigma(1 + \phi_B^2)}} \quad (14a,b)$$

High accuracy is guaranteed here by solving the frequencies $\tilde{\omega}_a$, $\tilde{\omega}_m$ for $K=39$, which means that 20 symmetric free-free plain beam flexural modes were considered. Now, for the equivalent two-degree-of-freedom system in Fig. 1b, one can write the attachment point receptance as (Kidner & Brennan, 1997):

$$r_{AA}(\omega)|_{2\text{-DOF}} = \frac{\omega_a^2 - \omega^2}{m_{a,red}\omega^2 \left\{ \omega^2 - \left(1 + m_{a,eff}/m_{a,red}\right)\omega_a^2 \right\}} \tag{15}$$

where

$$m_{a,eff} = Rm_a, \quad m_{a,red} = (1 - R)m_a, \quad m_a = (1 + \sigma)m_b \tag{16a-c}$$

The non-zero resonance of the function in eq. (15) is given by:

$$\omega_m|_{2\text{-DOF}} = \omega_a \sqrt{1 + m_{a,eff}/m_{a,red}} \tag{17}$$

For equivalence, $\omega_m|_{2\text{-DOF}} = \omega_m$ in eq. (17). Hence, by substituting this condition and eqs. (16a,b) into eq. (17), an expression can be obtained for the proportion R of the total absorber mass m_a that is effective in vibration attenuation:

$$R(\tilde{x}, \sigma) = 1 - (\tilde{\omega}_a/\tilde{\omega}_m)^2 \tag{18}$$

...where $\tilde{\omega}_a$, $\tilde{\omega}_m$ are the roots of eqs. (12, 13). Also, from eq. (15) and eqs. (16), the non-dimensional attachment point receptance of the equivalent system can be written as:

$$\tilde{r}_{AA}(\tilde{\omega}, \tilde{x}, \sigma)|_{2\text{-DOF}} = m_b \omega_1^2 r_{AA}(\omega)|_{2\text{-DOF}} = \frac{\tilde{\omega}_a^2 - \tilde{\omega}^2}{(1 + \sigma)\tilde{\omega}^2 \left\{ (1 - R)\tilde{\omega}^2 - \tilde{\omega}_a^2 \right\}} \tag{19}$$

The equivalent two-degree-of-freedom model is verified in Fig. 17 against the exact theory governing the actual (continuous) ATVA structures of Fig. 16 for $\sigma=5$ and two given settings $\tilde{x}=0.25, 0.5$. For each setting of \tilde{x} the corresponding values of $\tilde{\omega}_a$ and R were calculated using eqs. (12, 13, 18) and used to plot the function $\tilde{r}_{AA}(\tilde{\omega}, \tilde{x}, \sigma)|_{2\text{-DOF}}$ in eq. (19). Comparison with the exact receptance $\tilde{r}_{AA}(\tilde{\omega}, \tilde{x}, \sigma)$ (computed from eqs. (9) and (11)) shows that the equivalent two-degree-of-freedom system is a satisfactory representation of the actual systems in Fig. 16 over a frequency range which contains the operational frequency of the ATVA ($\omega = \omega_a$).

Next, using eqs. (12, 13, 18), the variations of ω_a and R with ATVA setting \tilde{x} for various fixed values of σ are investigated for both types of ATVA in Fig. 16. The resulting characteristics are depicted in Fig. 18. With reference to Fig. 18a, it is evident that, as σ is increased, the tuning frequency characteristics of both types of ATVA approach each other. Moreover, for $\sigma \geq 1$, both types of ATVA give roughly the same overall useable variation in ω_a relative to $\omega_a|_{\tilde{x}=1}$. The moveable-supports ATVA characteristics in Fig. 18a have a peak (which is more prominent for lower σ values) that gives the impression of a greater variation in ω_a than the moveable-masses ATVA. However, this is a “red herring” since

these peaks coincide with a stark dip to zero in the effective mass proportion R of the moveable-supports ATVA, as can be seen in Fig. 18b. These troughs in R are explained by the fact that, for given σ , the free body resonance ω_m of the moveable-supports ATVA (i.e. the resonance of the free-free beam with central mass attached) is fixed (i.e. independent of \tilde{x}), as can be seen from Figs. 17c,d. Hence, the nodes of the associated mode-shape are fixed in position so that when the setting \tilde{x} is such that the attachment points A of the moveable-supports ATVA coincide with these nodes, this ATVA becomes totally useless (i.e. attenuation $D=0$, eq. (7)).

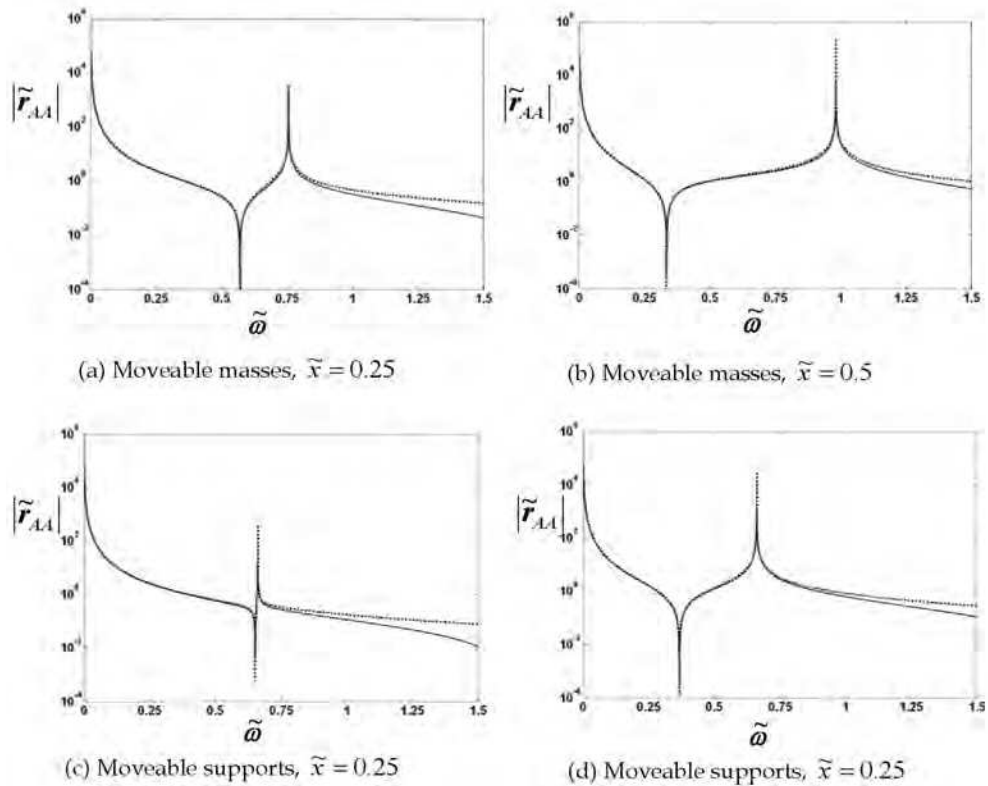


Fig. 17. Verification of equivalent two-degree-of-freedom model - non-dimensional attachment point receptance plotted against non-dimensional excitation frequency for two settings of the ATVAs in Figure 3 with $\sigma = 5$: exact, through eqs. (9) and (11) (—); equivalent 2-degree-of-freedom model, from eq. (19) (.....)

The moveable-masses ATVA does not suffer from this problem, and consequently has vastly superior effective mass characteristics, as evident from Fig. 18b. From eqs. (16a, b), one can rewrite the attenuation D in eq. (8) as:

$$D = \frac{1}{\eta_a} \left(\frac{R}{1 - R + M/m_a} \right) \tag{20}$$

It is evident from Fig. 18b and eq. (20) that the degree of attenuation D provided by a given moveable-supports ATVA in any given application undergoes considerable variability over its tuning frequency range, dipping to zero at a critical tuned frequency. On the other hand, the moveable-masses ATVA can be tuned over a comparable tuning frequency range while providing significantly superior vibration attenuation.

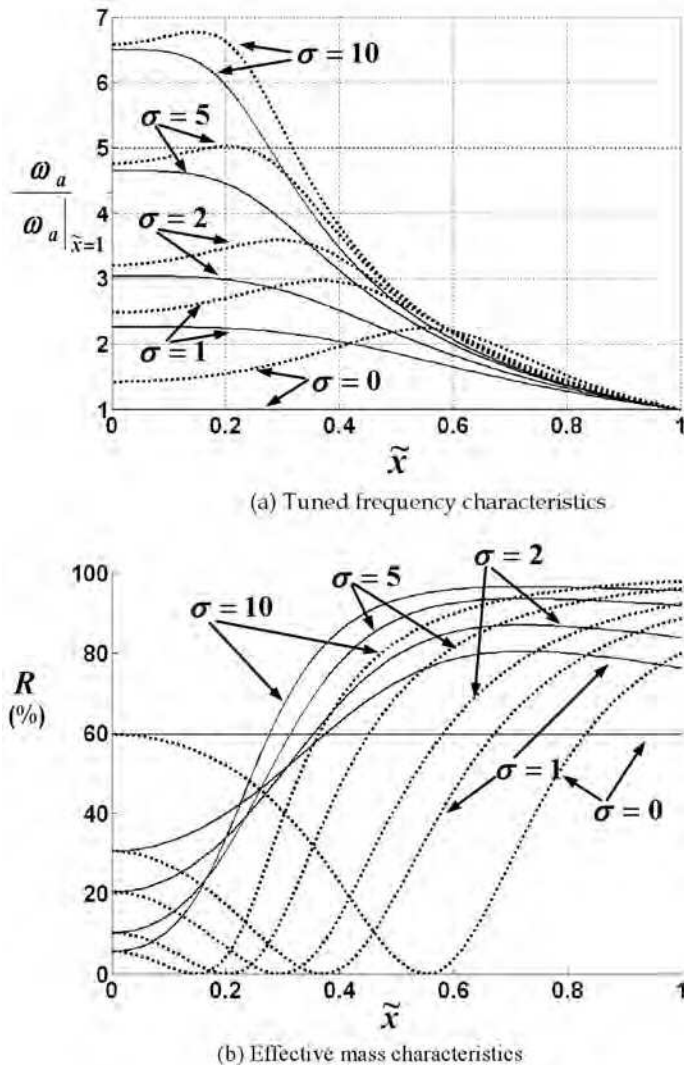


Fig. 18. Tuned frequency and effective mass characteristics for moveable-masses ATVA

4.2 Physical implementation and testing

Fig. 19 shows the moveable-masses ATVA with motor-incorporated masses that was built in (Bonello & Groves, 2009) to lend validation to the theory of the previous section and demonstrate the ATVA operation. The stepper-motors were operated from the same driver circuit board through a distribution box that sent identical signals to the motors, ensuring symmetrically-disposed movement of the masses. Each motor had an internal rotating nut that moved it along a fixed lead-screw. Each motor was guided by a pair of aluminium guide-shafts that, along with the lead-screw, made up the beam section.

The aim of Section 4.2.1 is to validate the theory of Section 4.1 whereas the aim of Section 4.2.2 is to demonstrate real-time ATVA operation.

4.2.1 Tuned frequency and effective mass characteristics

In these tests a random signal v was sent to the electrodynamic shaker amplifier and for each fixed setting \tilde{x} the frequency response function (FRF) H_{Av} relating \ddot{y}_A to v , and the FRF T_{BA} relating \ddot{y}_B to \ddot{y}_A (i.e. the transmissibility) were measured. Fig. 20a shows H_{Av} for different settings. The tuned frequency ω_a of the ATVA is the anti-resonance, which coincides with the resonance in T_{BA} . Fig. 20b shows that, at the anti-resonance, the cosine of the phase of T_{BA} is approximately zero. This is an indication that the absorber damping η_a (Fig. 1b) is low (Kidner et al., 2002). Hence, just like other types of ATVA e.g. (Rustighi et al., 2005, Bonello et al., 2005, Kidner et al., 2002), the cosine of the phase Φ between the signals \ddot{y}_A and \ddot{y}_B can be used as the error signal of a feedback control system for the ATVA under variable frequency harmonic excitation (Section 4.2.2). It is noted that this result is in accordance with the two-degree-of-freedom modal reduction of the ATVA and, additionally, it could be shown theoretically that the cosine of the phase between \ddot{y}_A and the signal \ddot{y}_Q at any other arbitrary point Q on the ATVA would also be zero in the tuned condition.

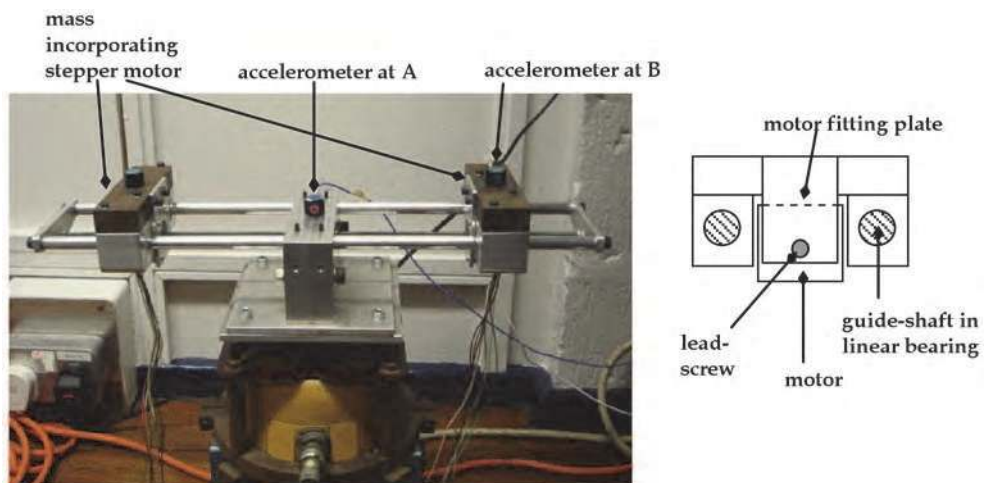


Fig. 19. Moveable-masses ATVA demonstrator mounted on electrodynamic shaker (inset shows motor-incorporated mass and ATVA beam cross-section)

Using the FRFs of Fig. 20a and a lumped parameter model of the ATVA/shaker combination it was possible to estimate the effective mass proportion R of the ATVA for each setting \tilde{x} , using the analysis described in (Bonello & Groves, 2009). The estimates varied slightly according to the type of damping assumed for the shaker armature suspension. However, as can be seen in Fig. 21, regardless of the damping assumption, there is good correlation with the effective mass characteristic predicted according to the theory of the previous section. Fig. 22 shows the predicted and measured tuning frequency characteristic, which gives the ratio of the tuned frequency to the tuned frequency at a reference setting. The demonstrator did not manage to achieve the predicted 418 % increase in tuned frequency, although it managed a 255 % increase, which is far higher than other proposed ATVAs e.g. (Rustighi et al., 2005, Bonello et al., 2005, Kidner et al., 2002) and similar to the percentage increase achieved by the V-Type ATVA in (Carneal et al., 2004). The main reasons for a lower-than-predicted tuned frequency as \tilde{x} was reduced can be listed as follows: (a) the guide-shafts-pair and lead-screw constituting the “beam cross-section” (Fig. 19) would only really vibrate together as one composite fixed-cross-section beam in bending, as assumed in the theory, if their cross-sections were rigidly secured relative to each other at regular intervals over the entire beam length – this was not the case in the real system and indeed was not feasible; (b) shear deformation effects induced by the inertia of the attached masses at B and the reaction force at A became more pronounced as \tilde{x} was reduced; (c) the slight clearance within the stepper-motors. It is noted that the limitation in (a) was exacerbated by the offset of the centroidal axis of the lead-screw from that of the guide-shafts (inset of Fig. 19). Moreover, the limitations described in (a) and (b) are also encountered when implementing the moveable-supports design (Fig. 16b). It is also interesting to observe that, at least for the case studied, the divergence in Fig. 22 did not significantly affect the good correlation in Fig. 21.

4.2.2 Vibration control tests

Fig. 23 shows the experimental set-up for the vibration control tests. The shaker amplifier was fed with a harmonic excitation signal v of time-varying circular frequency ω and fixed amplitude and the ability of the ATVA to attenuate the vibration \ddot{y}_A by maintaining the tuned condition $\omega_a = \omega$ in real time was assessed. The frequency variation occurred over the interval $t_i < t < t_f$ and was linear:

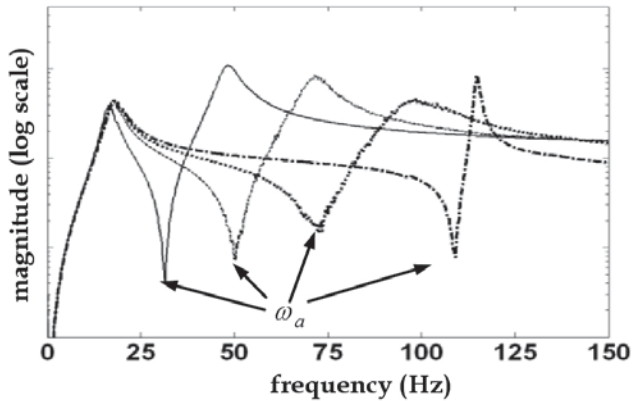
$$\omega = \begin{cases} \omega_i & t \leq t_i \\ \omega_i + \left[(\omega_f - \omega_i) / (t_f - t_i) \right] (t - t_i) & t_i < t < t_f \\ \omega_f & t \geq t_f \end{cases} \quad (21)$$

where ω_i, ω_f are the initial and final frequency values. The swept-sine excitation signal was hence as given by:

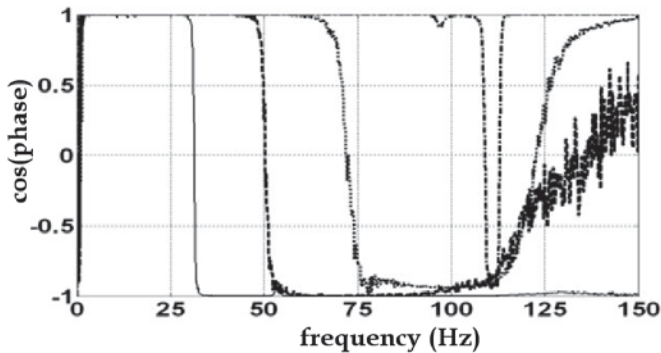
$$v = V \sin \theta, \quad \frac{d\theta}{dt} = \omega \quad (22a,b)$$

where, by substitution of (21) into (22b) and integration:

$$\theta = \begin{cases} \omega_i t & t \leq t_i \\ 0.5 \left[\frac{\omega_f - \omega_i}{t_f - t_i} \right] (t - t_i)^2 + \omega_i t & t_i < t < t_f \\ \omega_f t - 0.5 \left[\frac{\omega_f - \omega_i}{t_f + t_i} \right] & t \geq t_f \end{cases} \quad (23)$$



(a) FRF relating to \ddot{y}_A (output) to v (input)



(b) Cosine of phase of FRF relating to \ddot{y}_B (output) to \ddot{y}_A (input)

Fig. 20. Frequency response function measurements for different settings of ATVA of Fig. 19

The inputs to the controller were the signals \ddot{y}_A, \ddot{y}_B from the accelerometers. As discussed in Section 4.2.1, the instantaneous error signal fed into the controller was $e(t) = \cos \Phi$ and this was continuously evaluated from \ddot{y}_A, \ddot{y}_B by integrating their normalised product over a sliding interval of fixed length T_c , according to the following formula:

$$e(t) = \cos \Phi = \begin{cases} \frac{I_{AB}(t)}{\{I_{AA}(t)\}^{0.5} \{I_{BB}(t)\}^{0.5}} & (t \leq T_c) \\ \frac{I_{AB}(t) - I_{AB}(t - T_c)}{\{I_{AA}(t) - I_{AA}(t - T_c)\}^{0.5} \{I_{BB}(t) - I_{BB}(t - T_c)\}^{0.5}} & (t > T_c) \end{cases} \quad (24)$$

where

$$I_{AA}(t) = \int_0^t \ddot{y}_A(\tau) \ddot{y}_A(\tau) d\tau, \quad I_{BB}(t) = \int_0^t \ddot{y}_B(\tau) \ddot{y}_B(\tau) d\tau, \quad I_{AB}(t) = \int_0^t \ddot{y}_A(\tau) \ddot{y}_B(\tau) d\tau \quad (25a-c)$$

...and T_c was taken to be many times the interval Δ between consecutive sampling times of the data acquisition ($T_c = 100\Delta$ typically). Since the difference between the forcing frequency and the tuned frequency, $\omega - \omega_a$ is non-linearly related to $e(t)$, a non-linear control algorithm was necessary to minimise $|e(t)|$. Various such control algorithms for ATVAs have been proposed. For example, (Bonello et al., 2005) used a nonlinear P - D controller in which the voltage that controlled the piezo-actuators (Fig. 10) was updated according to a sum of two polynomial functions, one in e and the other in \dot{e} , weighted by suitably chosen constants P and D . (Kidner et al., 2002) formulated a fuzzy logic algorithm based on e to control the servo-motor of the device in Figure 12b. These algorithms were not convenient for the present application since they provided an analogue command signal to the actuator. In the present case, the available motor driver was far more easily operated through logic signals. Each motor had five possible motion states, respectively activated by five possible logic-combination inputs to the driver. Hence, the interval-based control methodology described in Table 1 was implemented, where the error signal computed by eq. (24) was divided into 5 intervals.

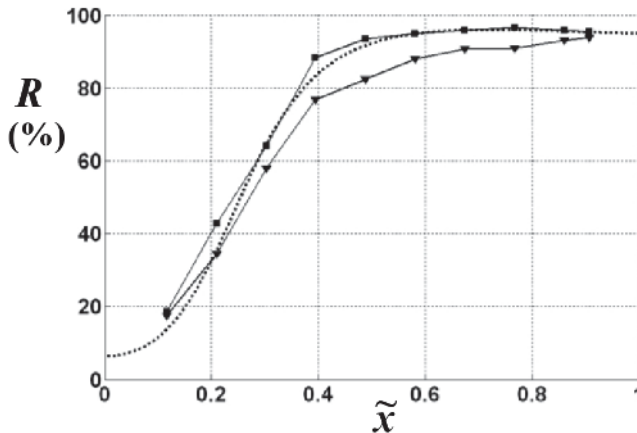


Fig. 21. Effective mass characteristics for prototype moveable masses ATVA: predicted (.....); measured, light damping assumption (—■—); measured, proportional damping assumption (—▼—)

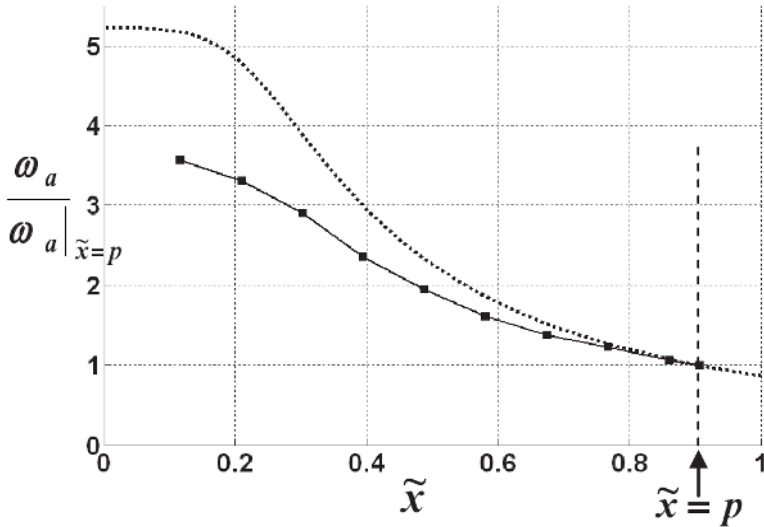


Fig. 22. Tuned frequency characteristic for prototype moveable masses ATVA: predicted (.....); measured (—■—)

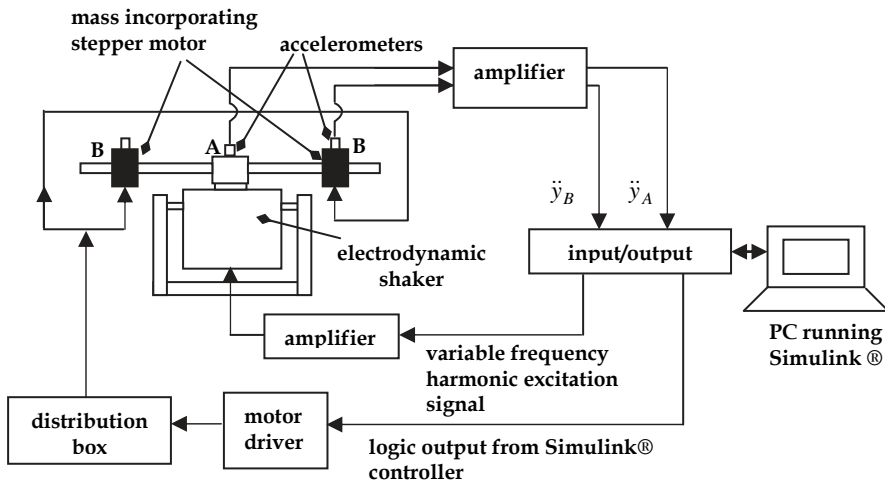


Fig. 23. Experimental set-up for vibration control test

The control system for the experimental set-up of Figure 23 was implemented in MATLAB® with SIMULINK® using the Real Time Workshop® and Real Time Windows Target® toolboxes.

Fig. 24 shows the results obtained for the frequency-sweep in Fig. 24a with the control system turned off and the ATVA tuned to a frequency of 56Hz. It is clear that at the instant

where the excitation frequency sweeps through 56 Hz, the amplitude of the acceleration \ddot{y}_A is at a minimum value and $\cos\Phi$ is approximately equal to zero (i.e. the ATVA is momentarily tuned to the excitation).

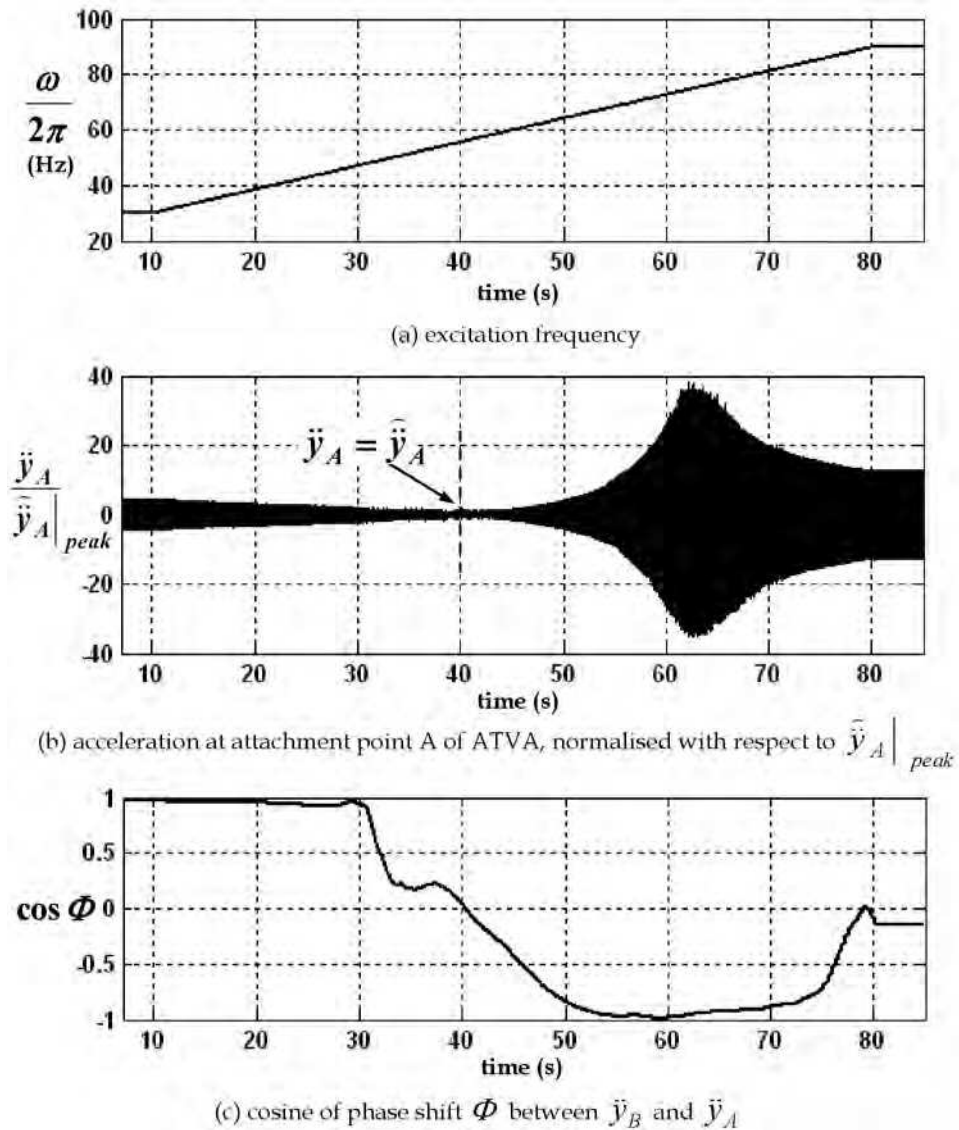
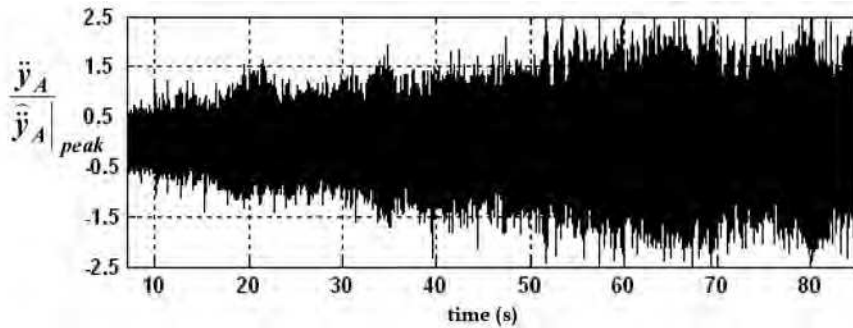


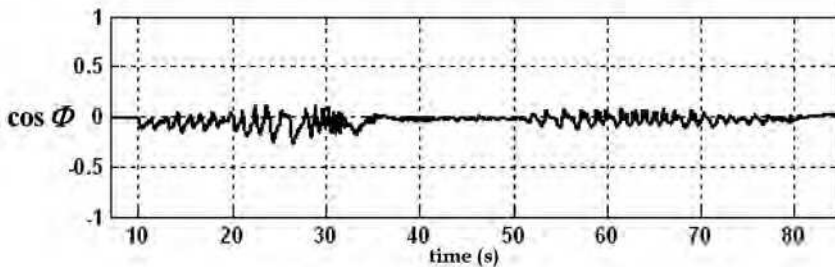
Fig. 24. Swept-sine test with controller turned off and ATVA tuned to a fixed frequency of 56 Hz ($\hat{y}_A|_{peak}$ is the amplitude of \hat{y}_A , the tuned acceleration at A at an excitation frequency of 56 Hz)

$\cos \Phi$	Motion State
$c_1 \leq \cos \Phi \leq 1$	Fast CW
$c_2 \leq \cos \Phi < c_1$	Slow CW
$-c_2 < \cos \Phi < c_2$	Stopped
$-c_2 \geq \cos \Phi > -c_1$	Slow CCW
$-c_1 \geq \cos \Phi \geq -1$	Fast CCW

Table 1. Interval-based control methodology for stepper-motor driver (CW: clockwise; CCW: counter-clockwise)



(a) acceleration at attachment point A of ATVA, normalised with respect to $\ddot{y}_A|_{peak}$ (defined in Figure 24)



(b) cosine of phase shift Φ between \ddot{y}_B and \ddot{y}_A

Fig. 25. Response to swept sine excitation (Figure 24a) with controller turned on and ATVA initially tuned to the excitation frequency (controller parameters in Table 1 are $c_1 = 0.04$, $c_2 = 0.02$).

Fig. 25 shows the response to the same frequency-sweep of Fig. 24a with the controller turned on. Prior to the start of the frequency-sweep at $t = 10$, the ATVA was allowed to tune itself, from whatever initial setting it had, to the prevailing excitation frequency of 30 Hz. As the sweep progressed, the controller returned the ATVA accordingly to reasonable accuracy, as illustrated in Fig. 25b. This resulted in minimised vibration over the entire sweep, as evident by comparing the scales of the vertical axes of Fig. 25a and 24b. However, it is evident from

Fig. 25a that the amplitude of the tuned vibration increases steadily over the frequency sweep between start and finish. Further studies revealed that this observed degradation in attenuation produced by the ATVA was due to the reduction in its effective mass proportion R as it retuned itself to a higher frequency, decreasing the effective mass ratio μ of the ATVA-shaker combination. This illustrated the importance of knowing the effective mass characteristic of a moveable-masses or moveable-supports ATVA. It is noted that the tests in this subsection (4.2.2) were made with an earlier version of the prototype wherein the ATVA beam came in two halves i.e. one separate lead-screw and a separate guide-shaft-pair for each symmetric half of the ATVA, each secured into the central block (see Fig. 19). The tests in section 4.2.1 were made with an improved version wherein the ATVA beam was one continuous piece, as in the theory (Fig. 16a) i.e. one long lead-screw and guide-shaft pair running straight through the central block, where they were tightly secured, ensuring a horizontal slope (see Fig. 19). Based on the validated results of Fig. 21, the observed degradation in attenuation in Fig. 25a is expected to be much less for the improved version.

5. Conclusion

This chapter started with a quantitative illustration of the basic design principles of both variants of the TVA: the TMD and the TVN. The importance of adaptive technology, particularly with regard to the TVN, was justified. The remainder of the chapter then focussed on adaptive (smart) technology as applied to the TVN. A comprehensive review of the various design concepts that have been proposed for the ATVA was presented. The latest ATVA concept introduced by the author, involving a beam-like ATVA with actuator-incorporated moveable masses, was then studied theoretically and experimentally. The variation in tuned frequency was shown to be significantly higher than most other proposed ATVAs and at least as high as that reported in the literature for the alternative moveable-supports beam ATVA design. Moreover, the analysis revealed that the moveable-masses beam concept offers significantly superior vibration attenuation relative to the moveable-supports beam concept, apart from constructional simplicity. Vibration control tests with logic-based feedback control demonstrated the efficacy of the device under variable frequency excitation. Current efforts by the author are being directed at introducing smart technology to TMDs.

6. References

- Bishop, R.E.D. & Johnson, D.C. (1960). *The Mechanics of Vibration*, Cambridge University Press, Cambridge, UK
- Bonello, P. & Brennan, M. J. (2001). Modelling the dynamic behaviour of a supercritical rotor on a flexible foundation using the mechanical impedance technique. *J. Sound and Vibration*, Vol.239, No.3, pp. 445-466
- Bonello, P.; Brennan, M. J. & Elliott, S. J. (2005). Vibration control using an adaptive tuned vibration absorber with a variable curvature stiffness element. *Smart Mater. Struct.*, Vol.14, No.5, pp. 1055-1065
- Bonello, P. & Groves, K.H. (2009). Vibration control using a beam-like adaptive tuned vibration absorber with actuator-incorporated mass-element. *Proceedings of the Institution of Mechanical Engineers - Part C: Journal of Mechanical Engineering Science.*, Vol.223., No.7, pp 1555-1567

- Brennan, M.J. (1997). Vibration control using a tunable vibration neutraliser. *Proc. IMechE Part C, Journal of Mechanical Engineering Science*, Vol.211, pp. 91-108
- Brennan, M.J. (2000). Actuators for active control – tunable resonant devices. *Applied Mechanics and Engineering*, Vol.5, No.1, pp. 63-74
- Brennan, M.J.; Bonello, P.; Rustighi, E., Mace, B.R. & Elliott, S.J. (2004a). Designs of a variable stiffness element for a tunable vibration absorber, *Proceedings of ICA2004 (The 18th International Congress on Acoustics)*, Vol.IV, pp. 2915-2918, Kyoto, Japan, 4-9 April, 2004
- Brennan, M.J.; Bonello, P.; Rustighi, E., Mace, B.R. & Elliott, S.J. (2004b). Designs of a variable stiffness element for a tunable vibration absorber, *Presentation given at ICA2004 (The 18th International Congress on Acoustics)*, Vol.IV, pp. 2915-2918, Kyoto, Japan, 4-9 April, 2004
- Carneal, J.P.; Charette, F. & Fuller, C.R. (2004). Minimization of sound radiation from plates using adaptive tuned vibration absorbers. *J. Sound and Vibration*, Vol.270, pp. 781-792
- Den Hartog, J.P. (1956). *Mechanical Vibrations*, McGraw Hill (4th Edition), New York, USA
- Ewins, D.J. (1984). *Modal Testing: Theory and Practice*, Letchworth: Research Student Press, UK
- Hong, D.P. & Ryu, Y.S. (1985). Automatically controlled vibration absorber. *US Patent No. 4935651*
- Kidner, M.R.F. & Brennan, M.J. (1999). Improving the performance of a vibration neutraliser by actively removing damping. *J. Sound and Vibration*, Vol.221, No.4, pp. 587-606
- Kidner, M. R. F. & Brennan, M. J. (2002). Variable stiffness of a beam-like neutraliser under fuzzy logic control. *Trans. of the ASME, J. Vibration and Acoustics*, Vol.124, pp. 90-99
- Ormondroyd, J. & den Hartog, J.P. (1928). Theory of the dynamic absorber. *Trans. of the ASME*, Vol. 50, pp. 9-22
- Long, T.; Brennan, M.J. & Elliott, S.J. (1998). Design of smart machinery installations to reduce transmitted vibrations by adaptive modification of internal forces. *Proceedings of the Institution of Mechanical Engineering - Part I: Journal of Systems and Control Engineering*, Vol.212, No.13, pp. 215-228
- Longbottom, C.J.; Day M.J. & Rider, E. (1990). A self tuning vibration absorber. *UK Patent No. GB218957B*
- Park, C.H. (2003). Dynamics modelling of beams with shunted piezoelectric elements. *J. Sound and Vibration*, Vol.268, pp. 115-129
- Rustighi, E.; Brennan, M.J. & Mace, B.R. (2005). A shape memory alloy adaptive tuned vibration absorber: design and implementation. *Smart Mater. Struct.*, Vol.14, No.1, pp. 19-28
- von Flotow, A.H.; Beard, A.H. & Bailey, D. (1994). Adaptive tuned vibration absorbers: tuning laws, tracking agility, sizing and physical implementation, *Proc. Noise-Con 94*, pp. 81-101, Florida, USA, 1994



Vibration Analysis and Control - New Trends and Developments

Edited by Dr. Francisco Beltran-Carbajal

ISBN 978-953-307-433-7

Hard cover, 352 pages

Publisher InTech

Published online 06, September, 2011

Published in print edition September, 2011

This book focuses on the important and diverse field of vibration analysis and control. It is written by experts from the international scientific community and covers a wide range of research topics related to design methodologies of passive, semi-active and active vibration control schemes, vehicle suspension systems, vibration control devices, fault detection, finite element analysis and other recent applications and studies of this fascinating field of vibration analysis and control. The book is addressed to researchers and practitioners of this field, as well as undergraduate and postgraduate students and other experts and newcomers seeking more information about the state of the art, challenging open problems, innovative solution proposals and new trends and developments in this area.

How to reference

In order to correctly reference this scholarly work, feel free to copy and paste the following:

Philip Bonello (2011). Adaptive Tuned Vibration Absorbers: Design Principles, Concepts and Physical Implementation, *Vibration Analysis and Control - New Trends and Developments*, Dr. Francisco Beltran-Carbajal (Ed.), ISBN: 978-953-307-433-7, InTech, Available from: <http://www.intechopen.com/books/vibration-analysis-and-control-new-trends-and-developments/adaptive-tuned-vibration-absorbers-design-principles-concepts-and-physical-implementation>

INTECH

open science | open minds

InTech Europe

University Campus STeP Ri
Slavka Krautzeka 83/A
51000 Rijeka, Croatia
Phone: +385 (51) 770 447
Fax: +385 (51) 686 166
www.intechopen.com

InTech China

Unit 405, Office Block, Hotel Equatorial Shanghai
No.65, Yan An Road (West), Shanghai, 200040, China
中国上海市延安西路65号上海国际贵都大饭店办公楼405单元
Phone: +86-21-62489820
Fax: +86-21-62489821

© 2011 The Author(s). Licensee IntechOpen. This chapter is distributed under the terms of the [Creative Commons Attribution-NonCommercial-ShareAlike-3.0 License](#), which permits use, distribution and reproduction for non-commercial purposes, provided the original is properly cited and derivative works building on this content are distributed under the same license.